

Temperature and thickness dependence of magnetic moments in NiO epitaxial films

D. Alders* and L. H. Tjeng

Solid State Physics Laboratory, Materials Science Centre, University of Groningen, Nijenborgh 4, 9747 AG Groningen, The Netherlands

F. C. Voogt and T. Hibma

Department of Chemical Physics, Materials Science Centre, University of Groningen, Nijenborgh 4, 9747 AG Groningen, The Netherlands

G. A. Sawatzky

Solid State Physics Laboratory, Materials Science Centre, University of Groningen, Nijenborgh 4, 9747 AG Groningen, The Netherlands

C. T. Chen

Synchrotron Radiation Research Center, Hsinchu Science-Based Industrial Park, Hsinchu 30077, Taiwan

J. Vogel,† M. Sacchi, and S. Iacobucci

Laboratoire pour l'Utilisation du Rayonnement Electromagnétique, Centre Universitaire Paris-Sud, Bât 209d, 91405, Orsay, France

(Received 17 December 1997)

We show that linear polarized x-ray-absorption spectroscopy can be used to measure the temperature and thickness dependence of magnetic moments in NiO thin films. We demonstrate that both the long-range order and the nearest-neighbor spin-spin correlations can be revealed. NiO (100) films with thicknesses of 5, 10, and 20 monolayers epitaxially grown on MgO (100) are studied. The Néel temperature is found to be strongly reduced from the bulk value even for the 20 monolayer film. [S0163-1829(98)11217-1]

I. INTRODUCTION

X-ray-absorption spectroscopy (XAS) and magnetic x-ray dichroism (MXD) have developed in the last decade to one of the most important techniques in the study of the electronic structure and magnetism in a wide range of materials. Since the theoretical prediction^{1,2} of strong MXD and the experimental demonstration thereof,³ the technique has been applied to a large variety of problems in magnetism including rare-earth⁴⁻⁶ and transition metal⁷⁻⁹ ferromagnets, antiferromagnets,¹⁰⁻¹² paramagnets,¹³ thin films, and multilayers.^{8,14-16} The recent development of sum rules have opened the possibility of determining separately the spin and orbital contributions to the magnetic moment in the ground state.^{17,18} Many of the studies have dealt with core to valence transitions involving strongly atomic like $3d$ open shells for the transition metals and $4f$ shells for the rare earths such as the $L_{2,3}$ and $M_{4,5}$ edges, respectively. These core to valence transitions show by far the largest dichroic effects and the line shapes are very well described by atomic multiplet theory.^{19,20} As far as XAS and MXD experiments are concerned, the main influence of solid-state effects is to lower the point-group symmetry of the $3d$ or $4f$ ion which can be included effectively in terms of crystal-field splittings.²¹ This renormalized atomic approach seems to work very well in describing many details of the XAS line shape and is used very successfully in the interpretation of MXD studies, especially for very ionic materials. More recently also, the spectra of more covalent materials can be well reproduced by including explicitly the hybridization of the $3d$ or $4f$ orbitals with surrounding ligands.²²

Another influence of the solid state is, of course, the pres-

ence of interatomic superexchange interactions. These cause long-range magnetic order and therefore influence the interatomic spin-spin correlation functions. In magnetically ordered materials these interactions result in spontaneous atomic magnetic moments (\mathbf{M}) whose temperature dependence is a measure of the long-range magnetic order parameter. Utilizing circularly polarized light, the temperature and field dependence of magnetic moments in ferromagnets can be measured via the magnetic circular dichroism (MCD) in the photoabsorption spectra, since MCD is sensitive to the expectation value of the local magnetic moment $\langle \mathbf{M} \rangle$. MCD will vanish for antiferromagnets, but it has been shown theoretically² and experimentally¹⁰⁻¹² that, using linearly polarized light, a magnetic linear dichroic (MLD) signal can be observed for the magnetically ordered state since MLD is proportional to $\langle \mathbf{M}^2 \rangle$.

In all of the above-mentioned approaches, however, one has neglected the influence that direct interatomic exchange and superexchange might have on the XAS line shapes. Indeed at first glance this influence is expected to be small because the energy splitting involved is only at most 0.1 eV which is small compared to multiplet interactions of several eV's which dominate the line shape of the XAS spectrum. It is nevertheless worthwhile to investigate the possibility of such an influence more carefully,¹² because if the line shape is indeed dependent on the (super)exchange interaction, it will be related to the nearest-neighbor spin-spin correlation function since the exchange field felt by a central atom will be given by $J \langle \mathbf{S}_i \cdot \sum_j \mathbf{S}_j \rangle$. If detectable, this would then open up the possibility to measure also the nearest-neighbor spin-spin correlation function in addition to the long-range order parameter. In this paper we present a detailed study of the Ni

$L_{2,3}$ -XAS in epitaxially grown NiO films and demonstrate the sensitivity of the XAS line shape to the nearest-neighbor spin-spin correlation function. In addition we also present results on the use of MLD to study the temperature and thickness dependence of local magnetic moments in antiferromagnetic thin films.

The paper is organized as follows. We start with a brief review of the crystal, electronic, and magnetic structure of NiO. We then discuss the theory of $L_{2,3}$ -XAS line shape including the influence of atomic multiplet structure, crystal-field splittings, and an external magnetic field acting only on the valence electron spin. In the final sections we describe the experiments carried out on NiO (100) films with thicknesses of 5, 10, and 20 monolayers epitaxially grown on MgO (100) and discuss the results.

II. CRYSTAL, ELECTRONIC AND MAGNETIC STRUCTURE OF NiO

NiO crystallizes in the rocksalt (NaCl) structure with a small orthorhombic distortion²³ in the antiferromagnetically ordered state. It is classified as an ionic electrical insulator with a charge-transfer gap of around 4 eV.²⁴ The divalent Ni ions are octahedrally coordinated by 6 O^{2-} ions in O_h point-group symmetry. The Ni ions are in a nominally $3d^8$ electronic configuration with polarity fluctuations strongly suppressed by the large on-site $3d$ - $3d$ atomic Coulomb interactions. The covalent mixing of Ni $3d$ -O $2p$ hybridization leads to a mixing in of about 7% $3d^9\bar{L}$ configurations where \bar{L} denotes a hole on the O $2p$ orbitals. This covalent mixing contributes to the crystal or ligand field splitting of the $3d$ orbitals and also is responsible for the Ni-O-Ni superexchange interactions. The crystal and ligand fields together with Hund's rule coupling stabilize a $3d^8(t_{2g}^6e_g^2; {}^3A_{2g})$ ground state with a spin of 1 and a strongly quenched orbital angular momentum. The first excited $3d^8$ multiplet is of the order of the crystal-field splitting higher in energy. Since distortions cannot split the ${}^3A_{2g}$ ground state, the lowering of the symmetry at the surface will not influence the spectral shape strongly.

The superexchange interaction via the Ni-O-Ni 180° bond is antiferromagnetic and leads to a type-II fcc antiferromagnetic order. Neutron and two-magnon Raman experiments determine a superexchange interaction of 19 meV,²⁵ and a bulk magnetic ordering temperature of $T_N=520$ K. The small contraction of the lattice along the $\langle 111 \rangle$ direction in the magnetically ordered state leads to a change in cell angle from 90° above T_N to $90^\circ 4'$ at 297 K and $90^\circ 6'$ at 78 K.²³ This small distortion gives rise to the presence of a small single-ion anisotropy and dipole-dipole interactions. Such a magnetocrystalline anisotropy favors ferromagnetic sheets of spin (111) planes which are antiferromagnetically stacked in $\langle 111 \rangle$ directions. In total there are 24 domains possible. Four principle so-called T domains correspond to the possible $\langle 111 \rangle$ directions which are themselves divided into three S domains corresponding to the three possible $\langle 11\bar{2} \rangle$ directions, and domains corresponding to a reversal of these spin directions. In the presence of all these domains no MLD is possible. However, for a thin film the influence of the surface and interface provide a net direction stabilizing certain domains relative to others. For example, for a (100) surface we

would expect the domains with the long axis \perp to the surface to have a different energy from those with the long axis in the plane of the surface. As we will show below, our results are consistent with a strong preference of domains with a long axis \perp to the surface.

III. THEORY OF XAS LINE SHAPE

The $L_{2,3}$ -XAS line shape is determined by the dipole allowed transition from the $2p^63d^N$ ground state to a subset of $2p^53d^{N+1}$ final states, with $N=8$ for a divalent Ni ion. To calculate the spectra, we will use the full atomic multiplet theory²⁶ and include the effects of the solid with effective crystal fields. The assumptions have proven to be very successful in describing XAS and MXD spectra of a large variety of materials, especially of the more ionic compounds. For the $2p^63d^N$ ground state, the Hamiltonian includes the F_{dd}^2 and F_{dd}^4 Slater integrals to account for intra-atomic $3d$ - $3d$ Coulomb and exchange interactions. The point charge and ligand contributions to the crystal field is included in a single parameter $10 Dq=1.65$ eV, which is the t_{2g}/e_g orbital splitting in O_h symmetry and is basically a fitting parameter. We also include the $3d$ spin-orbit coupling $\mathcal{H}_{LS}=\lambda L \cdot S$ with λ equal to its atomic value of 102 meV, although, as mentioned before, the $3d$ spin-orbit coupling is not really important for Ni^{2+} because of the large crystal field and the orbitally nondegenerate ${}^3A_{2g}$ ground state. For the $2p^53d^{N+1}$ final states, the Hamiltonian includes, in addition to the above, a core hole spin-orbit coupling term \mathcal{H}_{cLS} , and the F_{pd}^2 , F_{pd}^4 , G_{pd}^1 , and G_{pd}^3 Slater integrals to account for the $2p$ - $3d$ Coulomb and exchange interactions.

Different in our approach, is the introduction of a term describing, with realistic numbers, the (super)exchange interaction between the $3d$ electrons on atom i with a neighboring atom j via an intervening O^{2-} ion. This is introduced as an exchange field acting only on the $3d$ spin with a value of $\mathcal{H}_{EX}=\mathbf{B}_i^{ex} \cdot \mathbf{S}_j$, where $\mathbf{B}_i^{ex}=\sum_j J_{ij} \langle S_j \rangle$ is the local exchange field. This exchange field is quite different from an ordinary magnetic field since it does not act on the orbital part or on the core-hole states.

The XAS and MXD spectra are calculated using a modified version of Cowan's program,²⁶ in which the transition probabilities, Slater integrals, and spin-orbit interactions are calculated from self-consistent field Hartree-Fock atomic-wave functions. As usual, the Slater integrals are reduced to 80% of their Hartree-Fock values to account for intra-atomic configuration interactions and to be consistent with the experimental atomic optical spectra.²⁷

In Fig. 1 we compare the calculated isotropic XAS spectra with the experimental isotropic spectrum of a 20 monolayer film of NiO (100) collected at $T=298$ K. The spectra are dominated by the $2p$ core-hole spin-orbit coupling which splits the spectra roughly into two parts, namely the L_3 ($h\nu \approx 852$ eV) and L_2 ($h\nu \approx 870$ eV) white line regions, separated by about 18 eV. The line shape of the spectra depends strongly on the multiplet structure given by the various Coulomb and exchange interactions and crystal-field splittings. In Fig. 1(a), we show the XAS spectrum calculated for the Ni^{2+} ion in spherical symmetry, and in Fig. 1(b) in an octahedral crystal field of $10 Dq=1.65$ eV. A Lorentzian lifetime broadening of 0.3 and 0.45 eV has been included for the L_3

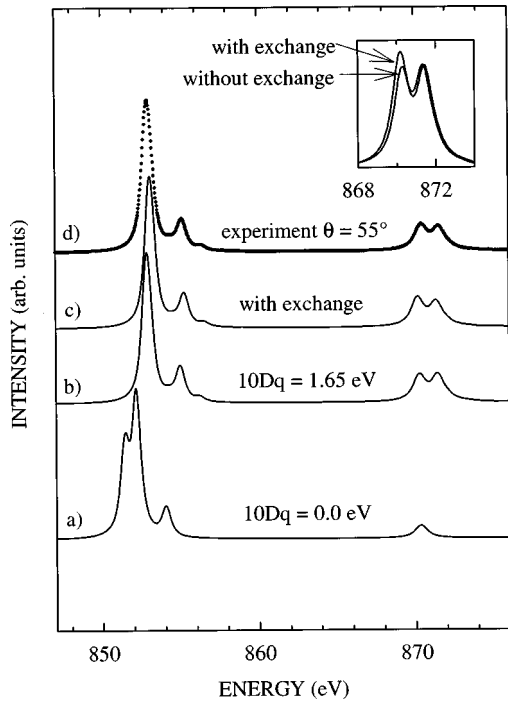


FIG. 1. $L_{2,3}$ -XAS of NiO. Calculated isotropic spectrum for a Ni^{2+} ion: (a) in spherical symmetry, (b) in octahedral symmetry with $10 Dq=1.65$ eV, and (c) in octahedral symmetry with $10 Dq = 1.65$ eV and an exchange field of 6×27 meV. A Lorentzian lifetime broadening of 0.3 and 0.45 eV has been included for the L_3 and L_2 edges, respectively. The experimental isotropic spectrum (d) is taken from a 20 monolayer NiO(100) film at $T=298$ K. The inset shows the calculated influence of the exchange field on the line shape of the L_2 white line in detail.

and L_2 edges, respectively. The influence of the crystal field on the spectra can be clearly seen, and the value used for $10 Dq$ reproduces apparently quite well the experimental spectrum depicted in Fig. 1(d).

In Fig. 1(c) we show the calculated spectrum in the presence of an exchange field, which acts only on the $3d$ spins, keeping the $10 Dq$ value of 1.65 eV. The exchange field felt by the Ni^{2+} ion is taken to be the total effective exchange field summed over the six nearest neighbors of 6×27 meV. From a comparison with Fig. 1(b), we can see that the influence of the exchange field on the isotropic spectrum is relatively small, which is not surprising since the exchange field is very much smaller than the various Coulomb interactions and crystal-field splittings. Nevertheless, this influence cannot be neglected: exchange fields introduce off-diagonal matrix elements between various multiplets in the final state, and will cause an appreciable amount of transfer of spectral weight, especially between those multiplets which are close in energy.¹² And indeed, this effect can be observed quite easily as a change in the line shape of the L_2 -edge spectrum: the inset of Fig. 1 shows that the applied exchange field transfers spectral weight from the higher lying peak at 871.5 eV to the lower lying peak at 870.2 eV of the double-peak structured L_2 white line. These peak intensity changes are of order 10%, and can be unambiguously detected in an experiment, since XAS spectra can be recorded with a noise-to-signal ratio and a reproducibility error of less than 0.5%. In fact, we now can see that the experimental L_2 white line can

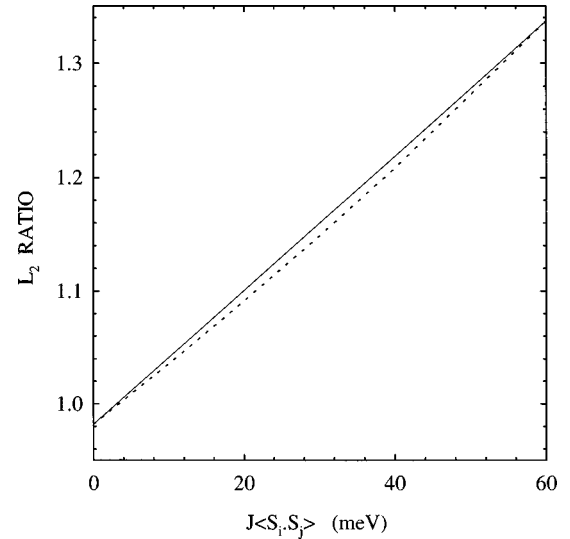


FIG. 2. Ratio of the two peaks in the isotropic Ni L_2 -XAS calculated for a Ni^{2+} ion in octahedral symmetry as a function of the exchange field $6 \times J \langle \mathbf{S}_i \cdot \mathbf{S}_j \rangle$. The calculated function is given by the dotted line and is compared to a linear curve given by the solid line. The almost perfect linearity of the calculated function makes this ratio to be a direct measure of the nearest-neighbor spin-spin correlation function.

be reproduced even better. We note that the exchange interaction required to simulate the spectrum is about 6×27 meV, which is higher than the ground-state value of 6×19 meV. As pointed out in an earlier paper,^{12,28} for the orbitally degenerate case, the influence of the exchange field is visible only for the final state, so it is this field and not the ground-state exchange field which is measured.

To facilitate the extraction of information concerning the local exchange field, we will now look for a characteristic signature in the XAS spectrum which has a simple relationship with the exchange field. A natural choice of course, is to take the ratio between the two peaks of the L_2 spectrum as described above. We calculate this ratio as a function of the magnitude of the exchange energy and the results are shown in Fig. 2. We find an almost perfect linear relationship, so that this ratio can indeed provide a straightforward measure of the exchange field, which in turn is directly related to the nearest-neighbor spin-spin correlation function, since the exchange field is given by $J \langle \mathbf{S}_i \cdot \mathbf{S}_j \rangle$. Note that we have used an exchange field which acts on the $3d$ spin only, and that a magnetic field will give a different relationship.

All the above spectra are isotropic, i.e., calculated for unpolarized light. This demonstrates that exchange fields and nearest-neighbor spin-spin correlation functions are measurable even without the use of polarization-dependent effects. If a material is magnetically ordered, then an XAS study using linearly polarized light can provide another opportunity, namely the measurement of the long-range order parameter. The dependence of the XAS spectrum on the angle θ between the polarization vector and the easy direction of the magnetic moment can be expressed as

$$I_{M_S}(\omega, \theta, J) = I^{(0)}(\omega) + \delta I_{M_S}^{(0)}(\omega, J) + (3 \cos^2 \theta - 1) I_{M_S}^{(2)}(\omega, J), \quad (1)$$

where ω is the photon energy and J is the effective exchange parameter. $I^{(0)}(\omega)$ is the isotropic spectrum in the absence of an exchange field, and $\delta I_{M_S}^{(0)}(\omega, J)$ represents the change in it due to the presence of an effective exchange field, thereby probing the nearest-neighbor spin-spin correlation function. The angle-dependent term $(3 \cos^2 \theta - 1) I_{M_S}^{(2)}(\omega, J)$ is proportional to the expectation value $\langle M_S^2 - \frac{1}{3} S(S+1) \rangle$ in the ground state,² and this MLD effect in the XAS therefore measures the long-range order parameter. To measure the nearest-neighbor spin-spin correlation function, it is most convenient to take the XAS spectrum at the magic angle, for which the $(3 \cos^2 \theta - 1)$ term vanishes. The sum over M_S of $\delta I_{M_S}^{(0)}(\omega, J)$ and of $I_{M_S}^{(2)}(\omega, J)$ are both zero, and so, at high temperatures, one retains only the exchange independent part of the isotropic spectrum $I^{(0)}(\omega)$.

IV. EXPERIMENT

The XAS experiments were performed at the AT&T Bell Laboratories Dragon beamline²⁹ at the National Synchrotron Light Source. The degree of linear polarization was measured to be $\approx 98.5\%$. The spectra were recorded using the total electron yield method and the accuracy of the angle definition is estimated to be within 1° . Part of the data (Fig. 7) have been recorded at the SA-22 beamline³⁰ of the LURE Super-ACO storage ring in Orsay, France.

Preparation of the samples were carried out at the University of Groningen. The thin NiO films were epitaxially grown, in a layer-by-layer fashion, on a single-crystal MgO (100) with NO_2 as an oxidizing agent, using a method described previously.³¹ Both NiO and MgO exhibit the face-centered-cubic rocksalt (NaCl) crystalline structure, with lattice constants of 4.176 and 4.212 Å, respectively, resulting in a 0.85% lattice mismatch. Films with 5, 10, and 20 monolayer thicknesses were made, and the thickness and sample characterization was done by reflection high-energy electron diffraction. After the preparation, the samples were taken out of the UHV chamber and transported to the synchrotron facility. This can be done without damaging the properties of the NiO thin films, since the NiO(100) surface is known to be very inert,³² e.g., a NiO(100) surface exposed to air still shows a low-energy electron-diffraction pattern. In addition, XAS in total electron-yield mode is a relatively bulk-sensitive detection technique with a probing depth of more than 50 Å for wide band-gap insulators like NiO.

V. RESULTS AND DISCUSSION

In Fig. 3 we show the Ni L_2 -XAS spectrum of a 20 monolayer NiO(100) film measured at room temperature as a function of the angle θ between the polarization vector of the light and the (100) surface normal. For clarity, the spectra are normalized at the first peak of the double-peak structured L_2 white line (if normalized to the incoming photon flux, the integrated intensity of the two peaks is a constant). The spectra exhibit clearly a very strong polarization dependence. The linear dichroic effect, taken as the change in the ratio between the two peaks, is of the order of 40%.

To investigate the origin of the linear dichroism, we measured the temperature dependence of the Ni L_2 -edge at nor-

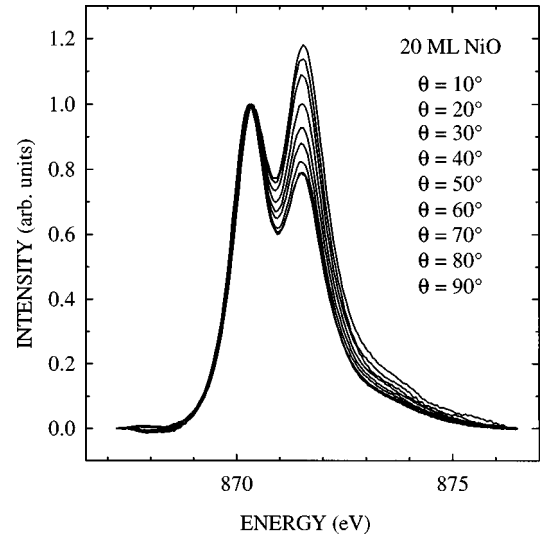


FIG. 3. Polarization dependence of the Ni L_2 -XAS of a 20 monolayer NiO(100) film at $T = 298$ K. θ is the angle between the (100) surface normal and the electric vector of the linearly polarized light. The spectra are normalized at the first peak of the L_2 -edge spectrum. Strong linear dichroism can be observed.

mal incidence of the light, i.e., $\theta = 90^\circ$. The data are shown in Fig. 4. The temperature dependence of the XAS line shape is very strong, with changes in peak intensities of the order of 25%. It is remarkable that above $T = 473$ K the temperature dependence seems to disappear completely, suggesting that the observed linear dichroic effect is of magnetic origin and that the temperature around 473 K can be identified as the Néel temperature of this NiO film.

In Fig. 5 we show a more extensive set of polarization and temperature-dependent data of the Ni L_2 -XAS, represented again in terms of the ratio between the two peaks of the L_2 white line. Reproducibility is demonstrated by the two sets of measurements at room temperature indicated by open and marked circles obtained before and after, respectively, heating up to $T = 528$ K. It is important to note that the linear

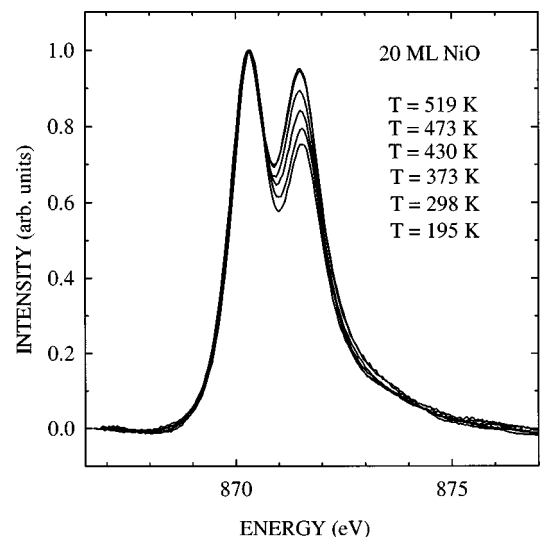


FIG. 4. Temperature dependence of the Ni L_2 -XAS of a 20 monolayer NiO(100) film taken at normal incidence of the linearly polarized light ($\theta = 90^\circ$).

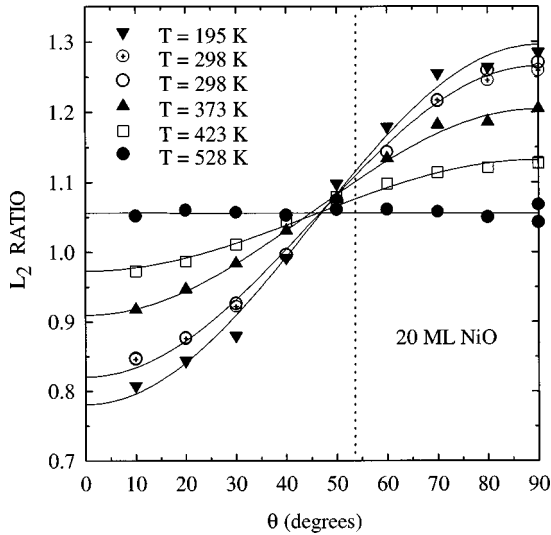


FIG. 5. Polarization and temperature dependence of the ratio of the two peaks in the Ni L_2 -XAS of a 20 monolayer NiO(100) film. θ is the angle between the (100) surface normal and the electric vector of the linearly polarized light. Reproducibility is demonstrated by the two sets of measurements at $T=298$ K, taken before and after heating up to 528 K, and indicated by open and marked circles, respectively. The set of full lines are fits to the data as described in the text, showing the $(3 \cos^2\theta - 1)$ angular dependence. Note the temperature dependence of the magic-angle data ($\theta = 54.7^\circ$) and the disappearance of the angle dependence above the Néel temperature ($T_N=470$ K).

dichroic effect completely disappears for the measurements taken at $T=528$ K. This demonstrates that the strong linear dichroic effect cannot be caused by the lowering of the point-group symmetry at the surface (D_{4h}), which is fully consistent with the fact that the 3A_2 state in O_h symmetry is not split in D_{4h} . For further analysis, we have also drawn in the figure a set of lines, which are fits to the experimental data and which have the $a(T) + b(T)(3 \cos^2\theta - 1)$ form as given by Eq. (1) for the theoretical angular dependence of the XAS spectrum. The good correspondence indicates that the observed linear dichroism is closely related to the long-range magnetic order parameter, since this also has the $(3 \cos^2\theta - 1)$ dependence.

Another remarkable result from Fig. 5 is that at the magic angle ($\theta=54.7^\circ$, $3 \cos^2\theta - 1=0$) the temperature dependence of the XAS spectra does not disappear. As explained in the theoretical section, we can relate these changes in the isotropic spectrum $[\delta I_{M_S}^{(0)}(\omega, J)]$ to changes in the exchange field. Therefore, the magic-angle data provide a direct measurement of the temperature dependence of the nearest-neighbor spin-spin correlation function. To further confirm this analysis, we have also carried out an XAS experiment on a NiO powder sample at various temperatures, which should provide the temperature dependence of a true isotropic spectrum, without being disturbed by any form of linear or circular dichroism. The results are shown in Fig. 6, together with the magic-angle data of the 20 monolayer film from Fig. 5. After a normalization of the temperatures to the proper Néel temperatures of the two systems, we can find an excellent correspondence between the two sets of data. This demonstrates clearly that XAS can provide direct information

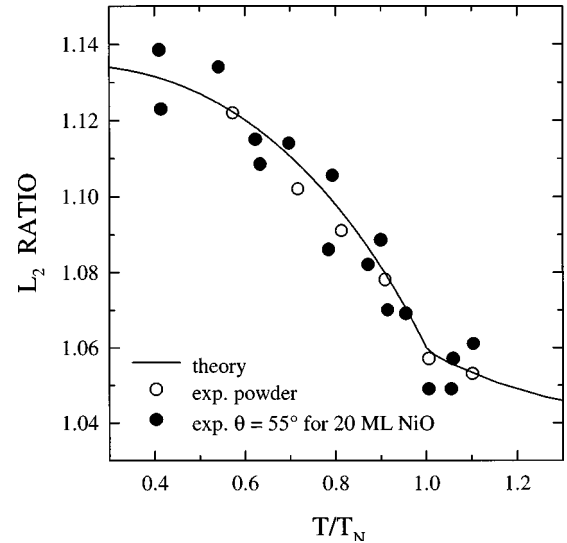


FIG. 6. Temperature dependence of the ratio of the two peaks in the isotropic XAS spectrum at the Ni L_2 edge. Filled circles: data taken from a 20 monolayer NiO(100) film ($T_N=470$ K) measured at the magic angle ($\theta=54.7^\circ$). Open circles: data taken from a NiO powder sample ($T_N=520$ K). The full line is a theoretical estimate for the temperature dependence of the nearest-neighbor spin-spin correlation function $\langle \mathbf{S}_i \cdot \mathbf{S}_j \rangle$, see text.

about the local exchange field and the nearest-neighbor spin-spin correlation function. To the best of our knowledge, there is no calculated result describing the nearest-neighbor spin-spin correlation function for an $S=1$ antiferromagnet. Therefore, we tentatively compare the data below T_N with a molecular field calculation using the Brillouin function ($S=1$), and the data above T_N with the short-range order parameter calculated using a constant coupling approximation³³ ($S=1/2$). The average of the local magnetic moment is then scaled at the Néel temperature to 0.295. The result is included in Fig. 6, and gives a surprisingly good fit to the data.

To verify that θ is the only geometrical parameter of interest for the observed MLD in the NiO films, and to relate the MLD to the magnetic domain structure of the thin film, we have also investigated the *azimuthal* angular dependence of the Ni L_2 -XAS. Figure 7 show the spectra taken at room temperature for a 30 monolayer NiO(100) film at normal incidence ($\theta=90^\circ$) for four different azimuthal angles $\varphi = -45^\circ, 0^\circ, 45^\circ$, and 90° . The absence of any azimuthal angular dependence can be clearly seen, suggesting strongly axial symmetry of the domains. This is not inconsistent with the domain structure of the thin film, in which, via the domain structure of bulk NiO, we can get the $\langle \pm 2 \pm 1 \pm 1 \rangle$ set of possible spin directions to form an easy axis \perp to the (100) surface.

In Fig. 8 we show a comparison between the experimental and theoretical angular dependence, at normal ($\theta=90^\circ$) and grazing ($\theta=15^\circ$) incidence. Simulation of the experimental spectra has been carried out with the atomic crystal-field calculations as outlined in the theoretical section, and with the same parameters as has been done for the isotropic spectrum in Fig. 1(c), i.e., $10 Dq=1.65$ eV and an effective exchange energy of 6×27 meV. A sum over the above-mentioned $\langle \pm 2 \pm 1 \pm 1 \rangle$ set of possible spin directions has been taken. The agreement between theory and experiment is very good,

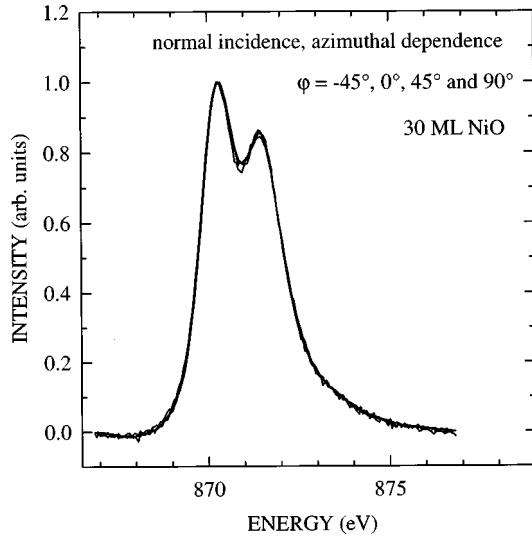


FIG. 7. Azimuthal angle dependence of the Ni L_2 -XAS of a 30 monolayer NiO(100) film at $T=298$ K. The spectra are taken at normal incidence of the linearly polarized light ($\theta=90^\circ$) for four different azimuthal angles ($\varphi=-45^\circ, 0^\circ, 45^\circ$, and 90°). The similarity of the spectra indicates axial symmetry.

especially for the Ni L_2 edge. The comparison for the Ni L_3 edge is not as good due to saturation effects,¹⁹ for which corrections have not been made here.

In Fig. 9 we show the experimental ratio of the two peaks in the Ni L_2 edge at normal incidence ($\theta=90^\circ$) as a function of temperature. Very recently, a similar temperature dependence has also been observed for bulk NiO, using x-ray mag-

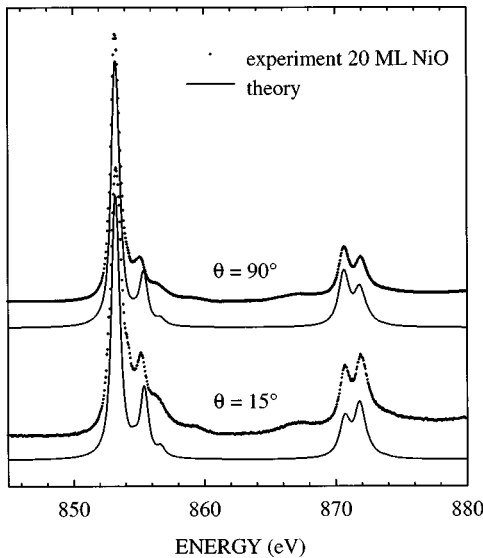


FIG. 8. Theoretical and experimental polarization dependence of the Ni $L_{2,3}$ -XAS of a NiO(100) thin film; (a) $\theta=90^\circ$: normal incidence of the linearly polarized light, i.e., electric vector in plane, and (b) $\theta=15^\circ$: grazing incidence, i.e., electric vector out of plane. Theoretical spectra (solid line) are calculated for a Ni^{2+} ion in octahedral symmetry with $10 Dq=1.65$ eV and an exchange field of 6×27 meV, and summed over the $\langle \pm 2, \pm 1, \pm 1 \rangle$ spin directions. A Lorentzian lifetime broadening of 0.3 and 0.45 eV has been applied for the L_3 and L_2 edges, respectively. Experimental spectra (dots) are taken from a 20 monolayer NiO(100) film measured at $T=298$ K.

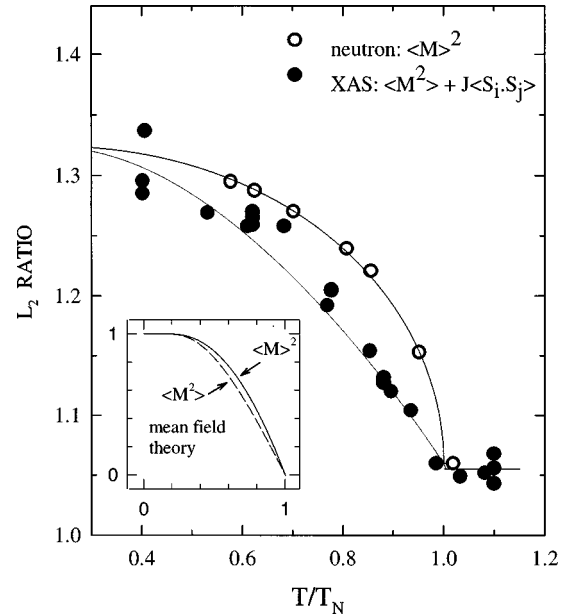


FIG. 9. Comparison of temperature-dependent XAS and neutron-diffraction data. Solid circles: the ratio of the two peaks in the Ni L_2 -XAS of a 20 monolayer NiO(100) film ($T_N=470$ K), measured at normal incidence ($\theta=90^\circ$). Open circles: magnetic moment obtained by neutron diffraction on bulk NiO ($T_N=520$ K) from Ref. 35. Thin lines are guides to the eye. XAS measures the quantity $\langle \mathbf{M}^2 \rangle + J \langle \mathbf{S}_i \cdot \mathbf{S}_j \rangle$, while neutron diffraction probes the quantity $\langle \mathbf{M} \rangle^2$. The inset shows, using a mean-field approach, the theoretically expected different behavior of $\langle \mathbf{M}^2 \rangle$ and $\langle \mathbf{M} \rangle^2$ with temperature, where both quantities have been normalized to 1 at $T/T_N=0$ and 0 at $T/T_N=1$.

netic scattering.³⁴ For comparison we also show in Fig. 9 the data from neutron-diffraction experiments,³⁵ in which $\langle \mathbf{M} \rangle^2$, i.e., the square of the local moment, is probed. Clearly this is quite different from our XAS results which, as pointed out above, are a measure of the sum of two contributions, namely a MLD part which is proportional to $\langle \mathbf{M}^2 \rangle$ and an exchange field part which scales with $J \langle \mathbf{S}_i \cdot \mathbf{S}_j \rangle$. It is interesting to note that theoretically one could already expect to find a different temperature dependence for $\langle \mathbf{M}^2 \rangle$ as compared to $\langle \mathbf{M} \rangle^2$. Within the molecular field theory, the first quantity is given² by $\langle \mathbf{M}^2 \rangle = J(J+1) + \langle \mathbf{M} \rangle \coth(1/2t)$, while the second quantity is given by $\langle \mathbf{M} \rangle^2 = J^2 B_J^2(J/t)$, where B_J is the Brillouin function and t is the reduced temperature $k_B T / g \mu_B H$. Their different behavior with temperature is shown in the inset of Fig. 9, where both curves have been normalized to 1 at $T/T_N=0$ and 0 at $T/T_N=1$.

Until now we have focused on the L_2 edge as far as the analysis of the experimental data are concerned. Yet, from the theoretical point of view, we would expect also a similar polarization and temperature-dependent behavior for the multiplets of the L_3 edge. Applying the same procedure as done for the L_2 edge, we plot in Fig. 10 the ratio between the L_3 main line and its shoulder for the 20 monolayer film at various temperatures and polarization angles. For high angles, i.e., close to normal incidence of the light, the data are quite similar to that of the L_2 edge as shown earlier in Fig. 5. For low angles, however, the L_3 -edge data are markedly different. This can be attributed to saturation effects, caused by the fact that, for strong absorbing lines such as the

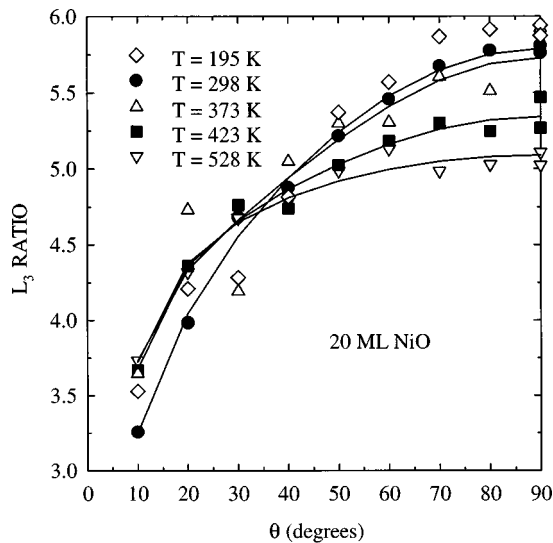


FIG. 10. Polarization and temperature dependence of the ratio of the two peaks in the Ni L_3 -XAS of a 20 monolayer NiO(100) film. θ is the angle between the (100) surface normal and the electric vector of the linearly polarized light. The set of full lines are fits to the data as described in the text, showing strong saturation effects, especially at grazing angles of incidence, on top of the $(3 \cos^2 \theta - 1)$ angular dependence.

L_3 main line, the effective absorption depth becomes comparable to the escape depth of the electrons detected in the total-yield method, especially at very grazing angles of incidence.¹⁹ The temperature and angle dependence can be fitted using the same function as for the L_2 edge, but now including a term describing the saturation effects: the full lines shown in the figure are fits of the form $a(T) + b(T)(3 \cos^2 \theta - 1)(d + \lambda_1 \sin \theta)/(d + \lambda_2 \sin \theta)$, where d is the electron escape depth and λ_1, λ_2 are the absorption length of the first and second peak, respectively, of the Ni L_3 edge.

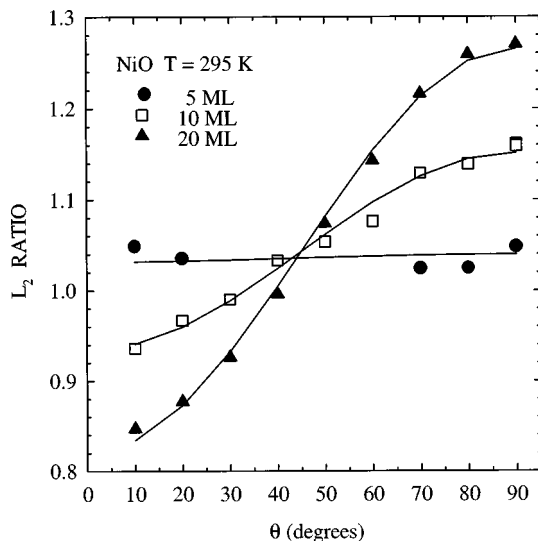


FIG. 11. Polarization and thickness dependence of the ratio of the two peaks in the Ni L_2 -XAS of NiO(100) thin films, taken at room temperature. θ is the angle between the (100) surface normal and the electric vector of the linearly polarized light. Note the disappearance of long-range order at room temperature for the 5 monolayer film.

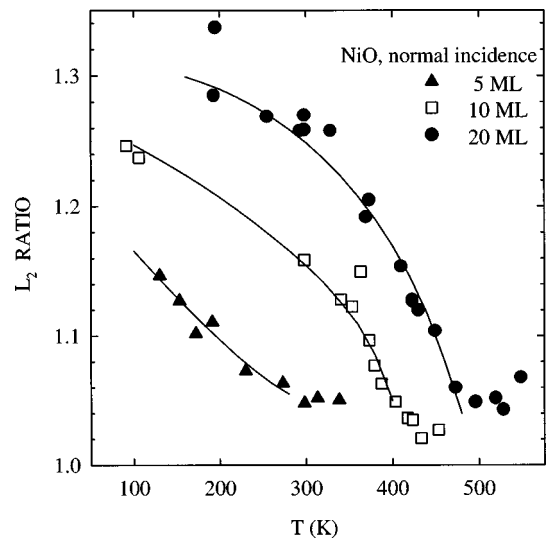


FIG. 12. Temperature and thickness dependence of the ratio of the two peaks in the Ni L_2 -XAS of NiO(100) thin films, taken at normal incidence. Néel temperatures of $T_N = 295, 430,$ and 470 K can be found for the 5, 10, and 20 monolayer films, respectively.

While the agreement is satisfactory, the analysis also shows that it is more elaborate to extract information concerning the long-range magnetic order and nearest-neighbor spin-spin correlation function from the Ni L_3 edge.

It is interesting now to use MLD to study the thickness dependence of the magnetic properties of NiO(100) thin films. In Fig. 11 we present the L_2 -edge data for a 5, 10, and 20 monolayer film, taken at room temperature. The linear dichroic effect for the 10 monolayer film is much reduced in comparison with the 20 monolayer film, while it has disappeared completely for the 5 monolayer film, indicating that this very thin film is in the paramagnetic state at room temperature. In Fig. 12 we now show the temperature dependence of the L_2 -edge peak ratio for the three NiO(100) films, all taken at normal incidence ($\theta = 90^\circ$). We can clearly observe that the Néel temperature is a strong function of the layer thickness, going from 520 K for the bulk to 470, 430, and 295 K for the 20, 10, and 5 monolayer films, respectively. This T_N dependence of antiferromagnetic films on the layer thickness has been observed before, both experimentally³⁶⁻³⁸ and theoretically.^{39,40} Using a mean-field approach, it has been found for the FeF₂ case that the bulk Néel temperature is reached to within 4% for a nine-layer film.³⁹ For the NiO case, however, we find reductions of 10% of the bulk Néel temperature for films as thick as 20 monolayers. This may be due to the different crystal structure. In the rocksalt (NaCl) structure, the nearest-neighbor (100) layers are not or hardly coupled via the superexchange interaction because of the 90° Ni-O-Ni bonds, while the next-nearest-neighbor layers are only coupled by one Ni-O-Ni 180° superexchange path. This means that the consecutive (100) layers are rather weakly coupled to each other. One may therefore expect that the bulk Néel temperature is reached only for fairly large NiO thicknesses, perhaps for about 30 or more monolayers.

VI. CONCLUSIONS

To conclude, we have carried out an XAS study at the Ni $L_{2,3}$ edges of NiO thin films, grown epitaxially on

MgO(100). We have shown that linear polarized XAS can be used to measure both the long-range magnetic order and the nearest-neighbor spin-spin correlation function. Temperature-dependent MLD measurements reveal that the Néel temperatures of the thin films are strongly reduced from the bulk value: $T_N=470$, 430, and 295 K for NiO films with thicknesses of 20, 10, and 5 monolayers, respectively. MLD can therefore be used to study the changes in magnetic properties for the transition from a three-dimensional to a two-dimensional antiferromagnetic system. Measurements at the magic angle ($\theta=54.7^\circ$, $3 \cos^2\theta-1=0$) show also a clear temperature dependence of the isotropic spectrum, which can be related to the temperature dependence of the nearest-neighbor spin-spin correlation function $J\langle\mathbf{S}_i\cdot\mathbf{S}_j\rangle$. This finding is further supported by the fact that the observed temperature dependence is identical to that of the XAS spectrum of a powder sample. XAS is therefore a promising tool to study the temperature-dependent short-range magnetic order,

not only below but also above the magnetic ordering temperature.

ACKNOWLEDGMENTS

We would like to thank B. T. Thole for fruitful discussions and J. C. Kappenburg for skillful technical assistance. This investigation was supported by the Netherlands Foundation for Chemical Research (SON), the Netherlands Foundation for Fundamental Research on Matter (FOM) with financial support from the Netherlands Organization for the Advancement of Pure Research (NWO). The National Synchrotron Light Source was supported by the U.S. Department of Energy under Contract No. DE-AC02-76CH00016. The research of L.H.T. was made possible by financial support from the Royal Netherlands Academy of Arts and Sciences.

*Present address: Philips Research Laboratories, Prof. Holstlaan 4, 5656 AA Eindhoven, The Netherlands.

†Present address: European Synchrotron Radiation Facility, Boîte Postale 220, 38043 Grenoble Cedex, France.

¹J. L. Erskine and E. A. Stern, *Phys. Rev. B* **12**, 5016 (1975).

²B. T. Thole, G. van der Laan, and G. A. Sawatzky, *Phys. Rev. Lett.* **55**, 2086 (1985).

³G. van der Laan, B. T. Thole, G. A. Sawatzky, J. B. Goedkoop, J. C. Fuggle, J. M. Esteve, R. Karnatak, J. P. Remeika, and H. Dabkowska, *Phys. Rev. B* **34**, 6529 (1986).

⁴G. Schütz, M. Knülle, R. Wienke, W. Wilhelm, W. Wagner, P. Kniele, and R. Frahm, *Z. Phys. B* **73**, 67 (1988).

⁵J. B. Goedkoop, B. T. Thole, G. van der Laan, G. A. Sawatzky, F. M. T. de Groot, and J. C. Fuggle, *Phys. Rev. B* **37**, 2086 (1988).

⁶F. Baudelet, C. Brouder, E. Dartyge, A. Fontaine, J. P. Kappler, and G. Krill, *Europhys. Lett.* **13**, 751 (1990).

⁷C. T. Chen, F. Sette, Y. Ma, and S. Modesti, *Phys. Rev. B* **42**, 7262 (1990).

⁸L. H. Tjeng, P. Rudolf, G. Meigs, F. Sette, C. T. Chen, and Y. U. Idzerda, *Proc. SPIE* **1548**, 160 (1991).

⁹P. Rudolf, F. Sette, L. H. Tjeng, G. Meigs, and C. T. Chen, *J. Magn. Magn. Mater.* **109**, 109 (1992).

¹⁰B. Sinkovic *et al.* have seen indications for MXD in BaCoF₄ from the temperature dependence of the dichroism of the Co $L_{2,3}$ edge near the Néel temperature. See B. Sinkovic, C. T. Chen, Y. Ma, F. Sette, and N. V. Smith, NLSL Annual Report 1989, p. 146 (unpublished); see also C. T. Chen and F. Sette, *Phys. Scr.* **T31**, 119 (1990).

¹¹P. Kuiper, B. G. Searle, P. Rudolf, L. H. Tjeng, and C. T. Chen, *Phys. Rev. Lett.* **70**, 1549 (1993).

¹²D. Alders, J. Vogel, C. Levelut, S. D. Peacor, M. Sacchi, T. Hibma, L. H. Tjeng, C. T. Chen, G. van der Laan, B. T. Thole, and G. A. Sawatzky, *Europhys. Lett.* **32**, 259 (1995).

¹³J. van Elp, S. J. George, J. Chen, G. Peng, C. T. Chen, L. H. Tjeng, G. Meigs, H.-J. Lin, Z. H. Zhou, M. W. W. Adams, B. G. Searle, and S. P. Cramer, *Proc. Natl. Acad. Sci. USA* **90**, 9664 (1993); S. J. George, J. van Elp, J. Chen, Y. Ma, C. T. Chen, J.-B. Park, M. W. W. Adams, B. G. Searle, F. M. F. de Groot, J. C. Fuggle, and S. P. Cramer, *J. Am. Chem. Soc.* **114**, 4426 (1992).

¹⁴L. H. Tjeng, Y. U. Idzerda, P. Rudolf, F. Sette, and C. T. Chen, *J.*

Magn. Magn. Mater. **109**, 288 (1992).

¹⁵Y. U. Idzerda, L. H. Tjeng, H.-J. Lin, C. J. Gutierrez, G. Meigs, and C. T. Chen, *Phys. Rev. B* **48**, 4144 (1993); *Surf. Sci.* **287/288**, 741 (1993).

¹⁶M. G. Samant, J. Stöhr, S. S. P. Parkin, G. A. Held, B. D. Hermsmeier, F. Herman, M. van Schilfgaarde, L.-C. Duda, D. C. Mancini, N. Wassdahl, and R. Nakajima, *Phys. Rev. Lett.* **72**, 1112 (1994).

¹⁷B. T. Thole, P. Carra, F. Sette, and G. van der Laan, *Phys. Rev. Lett.* **68**, 1943 (1992).

¹⁸P. Carra, B. T. Thole, M. Altarelli, and X. Wang, *Phys. Rev. Lett.* **70**, 694 (1993).

¹⁹B. T. Thole, G. van der Laan, J. C. Fuggle, G. A. Sawatzky, R. C. Karnatak, and J. M. Esteve, *Phys. Rev. B* **32**, 5107 (1985).

²⁰G. van der Laan and B. T. Thole, *Phys. Rev. B* **43**, 13 401 (1991).

²¹F. M. F. de Groot, Ph.D. thesis, University of Nijmegen, 1991.

²²A. Kotani, H. Ogasawara, K. Okada, B. T. Thole, and G. A. Sawatzky, *Phys. Rev. B* **40**, 65 (1989).

²³M. T. Hutchings and E. J. Samuelsen, *Phys. Rev. B* **6**, 3447 (1972).

²⁴G. A. Sawatzky and J. W. Allen, *Phys. Rev. Lett.* **53**, 2339 (1984).

²⁵R. E. Dietz, G. I. Parisot, and A. E. Meixner, *Phys. Rev. B* **4**, 2302 (1971).

²⁶R. D. Cowan, *The Theory of Atomic Structure and Spectra* (University of California Press, Berkeley, 1981).

²⁷C. E. Moore, *Atomic Energy Levels*, Natl. Bur. Stand. (U.S.) Circ. No. 467 (U.S. GPO, Washington, D.C., 1958), Pts. I–III.

²⁸M. A. van Veenendaal, D. Alders, and G. A. Sawatzky, *Phys. Rev. B* **51**, 13 966 (1995).

²⁹C. T. Chen, *Nucl. Instrum. Methods Phys. Res. A* **256**, 595 (1987); C. T. Chen and F. Sette, *Rev. Sci. Instrum.* **60**, 1616 (1989); C. T. Chen, *ibid.* **63**, 1229 (1992).

³⁰J. Vogel, Ph.D. thesis, University of Nijmegen, 1994.

³¹S. D. Peacor and T. Hibma, *Surf. Sci.* **301**, 11 (1994).

³²Recently we have also performed measurements on *in situ* grown NiO samples on MgO (100). The polarization dependence found was exactly the same as reported here for samples exposed to air.

³³P. W. Kastelijn and J. Kranendonk, *Physica (Amsterdam)* **22**, 367 (1956).

- ³⁴J. P. Hill, C.-C. Kao, and D. F. McMorrow, *Phys. Rev. B* **55**, R8662 (1997).
- ³⁵W. L. Roth, *Phys. Rev.* **111**, 772 (1958).
- ³⁶M. Takano, T. Terashima, Y. Bando, and H. Ikeda, *Appl. Phys. Lett.* **51**, 205 (1987).
- ³⁷C. A. Ramos, D. Lederman, A. R. King, and V. Jaccarino, *Phys. Rev. Lett.* **65**, 2913 (1990).
- ³⁸J. A. Borchers, M. J. Carey, R. W. Erwin, C. F. Majkrzak, and A. E. Berkowitz, *Phys. Rev. Lett.* **70**, 1878 (1993); M. J. Carey, A. E. Berkowitz, J. A. Borchers, and R. W. Erwin, *Phys. Rev. B* **47**, 9952 (1993); J. A. Borchers, M. J. Carey, A. E. Berkowitz, R. W. Erwin, and C. F. Majkrzak, *J. Appl. Phys.* **73**, 6898 (1993).
- ³⁹A. S. Carriço and R. E. Camley, *Phys. Rev. B* **45**, 13 117 (1992).
- ⁴⁰R. W. Wang and D. L. Mills, *Phys. Rev. B* **46**, 11 681 (1992).